Front. Med. 2025, 19(6): 1022−1035
https://doi.org/10.1007/s11684-025-1181-z

RESEARCH ARTICLE

Macrophage-derived semaphorin 7A drives atherosclerosis via the integrin β1/JNK/MSR1 axis

Fengchan Li[1,*], Haofu Ni[1,*], Fan Tang[1,*], Jiaxin Lyu[1], Lili Wu[2], Lijie Ren[1], Qiongyu Lu[1], Shouming Zhao[6], Chaojun Tang (✉)[1,3,4,5,6], Li Zhu (✉)[2,3,4,5]

[1]Cyrus Tang Medical Institute, Soochow University, Suzhou 215123, China; [2]Suzhou Ninth Hospital Affiliated to Soochow University, Soochow University, Suzhou 215200, China; [3]Collaborative Innovation Center of Hematology of Jiangsu Province, Soochow University, Suzhou 215123, China; [4]National Clinical Research Center for Hematologic Diseases, the First Affiliated Hospital of Soochow University, Suzhou 215006, China; [5]Suzhou Key Laboratory of Thrombosis and Vascular Biology, Soochow University, Suzhou 215123, China; [6]Depar tment of Cardiology, the First People's Hospital of Taicang, Taicang Affiliated Hospital of Soochow University; Soochow University, Suzhou 215400, China

Abstract **Atherosclerosis is a chronic inflammatory disease driven by pathological processes such as macrophage foam cell formation. Semaphorin 7A (SEMA7A) is an immunoregulatory signaling molecule known to modulate immune responses and cellular adhesion. However, the contribution of macrophage-derived SEMA7A to atherogenesis has yet to be fully elucidated. In this study, we analyzed gene expression profiles of human mononuclear cells from the Gene Expression Omnibus (GEO) database and revealed highly expressed SEMA7A and its receptor integrin β1 in macrophages. The upregulation of SEMA7A and integrin β1 was also observed during the differentiation of THP-1 monocytes into macrophages. Mice with macrophage-specific deletion of *Sema7a* showed a 57.2% reduction in atherosclerotic lesion size and improved plaque stability in atherosclerosis mouse model compared to control mice. Mechanistically, macrophage SEMA7A promoted the expression of macrophage scavenger receptor 1 (MSR1) and lipid uptake mediated by integrin β1 and downstream JNK signaling pathway in macrophages. Notably, pharmacological inhibition of integrin β1 with integrin receptor antagonist GLPG0187 effectively suppressed atherosclerosis progression. These findings identify macrophage-derived SEMA7A as a key driver of atherosclerosis through a novel integrin β1/JNK/MSR1 axis, providing potential targets for the prevention and treatment of atherosclerosis.**

Keywords atherosclerosis; macrophage; SEMA7A; lipid uptake

Introduction

Atherosclerosis is the leading cause of cardiovascular disease (CVD), which has surpassed cancer and infectious diseases as the primary cause of death and disability worldwide [1]. The pathogenesis of atherosclerosis is a complex process involving multiple cell types and their intricate interactions. The key cell types include endothelial cells [2], smooth muscle cells [3], macrophages [4], foam cells [5], and T lymphocytes [6], all of which contribute to critical processes such as plaque formation, inflammation, fibrous cap development, and lipid deposition. Among these factors, lipid deposition plays a central role not only in the initiation of atherosclerosis but also in increasing the risk of plaque rupture through mechanisms such as inflammation, lipid core formation, and fibrous cap destabilization, thereby increasing the likelihood of cardiovascular events. Therefore, elucidating the molecular mechanisms underlying intracellular lipid transport may identify key targets for the prevention and treatment of atherosclerosis.

Macrophages are multifunctional cells that contribute to all stages of atherosclerosis, from plaque initiation to rupture [7]. Following endothelial injury and increased vascular permeability, circulating monocytes are recruited to the intima, where they differentiate into macrophages [8]. Once within the intima, oxidized low-density

Received June 17, 2025; accepted August 27, 2025
Correspondence: Li Zhu, zl15195682930@126.com;
Chaojun Tang, zjtang@suda.edu.cn

*These authors contributed equally to this work.

lipoprotein (ox-LDL) derived from LDL cholesterol disrupts lipid metabolism in macrophages, triggering foam cell formation and the secretion of proinflammatory cytokines, thereby amplifying the inflammatory response [9,10]. The cluster of differentiation 36 (CD36) and macrophage scavenger receptor 1 (MSR1) have been identified as key regulators of lipid uptake in macrophages via receptor-mediated endocytosis [11]. However, the precise molecular mechanisms regulating CD36 and MSR1 expression in macrophages and their subsequent effects on lipid uptake remain poorly understood. Therefore, identifying molecules that regulate MSR1 and CD36 expression may reveal novel therapeutic targets for atherosclerosis.

Semaphorin 7A (SEMA7A) is a distinct member of the semaphorin class VII subfamily and is characterized by a membrane-bound glycosylphosphatidylinositol (GPI) anchor [12]. SEMA7A was initially identified in the nervous system for its role in axon growth and neuronal migration [12,13]. SEMA7A has since been implicated in various inflammation-related pathological processes, including multiple sclerosis [14,15], cancer [16,17], sepsis [18], obesity [19], and cardiovascular diseases [20,21]. Our recent studies showed that endothelial SEMA7A responds to disturbed flow, promoting leukocyte adhesion, angiogenesis, and endothelial-to-mesenchymal transition (EMT) via its receptor integrin β1-mediated signaling pathways [20,22,23]. In addition to endothelial cells, SEMA7A has been implicated in the regulation of other vascular and immune cell types. For instance, it has been reported to promote smooth muscle cell migration and proliferation [24]. In lymphocytes, SEMA7A modulates T cell-mediated inflammation and enhances cytokine production [25], indicating its broader immunoregulatory roles in vascular inflammation. Notably, elevated serum levels of SEMA7A were observed in patients with acute atherothrombotic stroke (AAS) [26] and acute aortic dissection (AAD) [27]. However, the role of macrophage SEMA7A in the development of atherosclerosis and the underlying mechanisms remain to be fully elucidated.

In this study, by analyzing the gene expression profile of human mononuclear cells from the Gene Expression Omnibus (GEO) database, we revealed significantly greater expression of SEMA7A and its receptor integrin β1 in macrophages than in monocytes. By generating macrophage-specific *Sema7a* knockout mice, we showed that deletion of macrophage *Sema7a* attenuated atherosclerotic plaque formation and enhanced plaque stability in $Ldlr^{-/-}$ mice. Further investigation revealed that SEMA7A promoted lipid uptake by macrophages through the integrin β1-mediated JNK/MSR1 signaling pathway and that pharmacological inhibition of integrin β1 suppressed atherosclerosis progression, providing potential therapeutic targets for atherosclerosis.

Materials and methods

Animals

The animal protocol for this study was approved by the Ethics Committee of Soochow University. *Sema7a*-flox ($Sema7a^{fl/fl}$) mice were generated by the CAM-SU Genomic Resource Center at Soochow University. Mouse strains, including $Sema7a^{-/-}$, $Ldlr^{-/-}$, and *LysM-Cre*, were obtained from Jackson Laboratory (Bar Harbor). To generate macrophage-specific *Sema7a*-knockout mice ($Sema7a^{\Delta M\phi}$), *Sema7a-flox* mice were crossed with *LysM-Cre* mice. To establish a Western diet (WD)-induced atherosclerosis mouse model, macrophage-specific *Sema7a*-knockout mice on an *Ldlr* knockout background were generated by crossing $Ldlr^{-/-}$ mice with $Sema7a^{\Delta M\phi}$ mice. All animal experiments were conducted under specific pathogen-free (SPF) barrier conditions and in strict accordance with the institutional guidelines of the Laboratory Animal Center at Soochow University.

Sudan IV staining

The $Sema7a^{\Delta M\phi}$ $Ldlr^{-/-}$ and control $Sema7a^{fl/fl}$ $Ldlr^{-/-}$ mice were maintained on a normal chow diet for the first 8 weeks, after which they were transitioned to a WD (HFHC, Dyets) for another 12 weeks. To quantify the atherosclerotic lesions, *en face* staining was performed on the aortas of $Sema7a^{\Delta M\phi}$ $Ldlr^{-/-}$ and $Sema7a^{fl/fl}$ $Ldlr^{-/-}$ mice following euthanasia as described previously [20]. Briefly, the entire aorta was carefully isolated and fixed overnight in 4% paraformaldehyde after heart perfusion with ice-cold phosphate-buffered saline (PBS). The aortas were subsequently rinsed in 70% ethanol for 5 min, stained with Sudan IV (S4261; Sigma–Aldrich, USA) for 15 min, destained with 80% ethanol for 3 min, washed, and stored in PBS. The aortas were then longitudinally opened along the ventral midline and pinned flat. Images of the entire aorta and carotid artery were captured via a stereo microscope (SZX16, Olympus, Japan) and analyzed with cellSens software.

Hematoxylin and eosin staining

The atherosclerotic aortic roots of $Ldlr^{-/-}$ $Sema7a^{\Delta M\phi}$ and $Ldlr^{-/-}$ $Sema7a^{fl/fl}$ mice were fixed with 4% paraformaldehyde overnight before paraffin embedding. Hematoxylin and eosin (HE) staining was performed via a Hematoxylin and Eosin Staining Kit (C0105, Beyotime, China) according to the manufacturer's protocol. Briefly, after deparaffinization, the tissues were stained with hematoxylin for 5 min, differentiated with 1% hydrochloric acid alcohol for 3 s, and then stained with eosin for 15 s. The tissues were then subjected to dehydration, clearing, and mounting in sequence.

Oil red O staining

The atherosclerotic aortic roots of *Ldlr*$^{-/-}$ *Sema7a*$^{\Delta M\phi}$ and *Ldlr*$^{-/-}$ *Sema7a*$^{fl/fl}$ mice were fixed in 4% paraformaldehyde overnight before dehydration. After dehydration, the aortic roots were embedded in optimal cutting temperature (O.C.T.) compound and stored at −80 °C. The frozen sections (8 μm) were stained with 0.5% propylene glycol solution prepared from oil red O powder (O104972, Aladdin) according to the manufacturer's protocol. Briefly, the frozen sections were placed into a staining jar containing 0.5% oil red O-propanediol solution, filtered with a 0.22 μm filter, and stained for 1 h. The sections were then counterstained with a counterstaining solution for 3 min, followed by mounting and upright microscopic examination. For cell staining, the cells were fixed with 4% paraformaldehyde, stained with 0.5% oil red O-propanediol solution for 30 min, and subsequently stained with hematoxylin staining solution (C0105, Beyotime, China) for 30 s. Finally, the cells were photographed via an inverted microscope.

Administration of GLPG0187

A mouse carotid atherosclerosis model was established via a combination of partial carotid artery ligation with an intravenous injection of AAV-mPCSK9^{DY} in 10-week-old male wild-type mice, which were maintained on a WD for the next two weeks [28]. An intravenous injection of GLPG0187 (2 mg/kg) was administered one day before the model was induced and every other day afterwards throughout this period.

Isolation of peritoneal macrophages

Peritoneal macrophages (PMs) were isolated as described previously [29]. PMs were isolated by intraperitoneally injecting 2.5 mL of 3% thioglycolate medium into the mice, followed by a 3-day feeding period in a SPF environment. After euthanasia by CO_2, the peritoneal cavity of each mouse was injected with 5 mL of ice-cold PBS containing 1.5% FBS to collect the lavage fluid. The peritoneal cells were then centrifuged at 1000 rpm for 5 min to pellet the cells. The cell pellet was resuspended in 1 mL of high-glucose DMEM supplemented with 10% FBS. The cells were cultured in a 10 cm dish for 2 h, and the adherent cells, which were identified as PMs, were collected. To induce lipid uptake in PMs, cells were first stimulated with 100 ng/mL IFN-γ + 100 ng/mL LPS for 24 h, followed by treatment with ox-LDL (YB-002, Yiyuanbiotech, China) at a final concentration of 50 μg/mL for 48 h.

Culture of bone marrow-derived macrophages

Bone marrow-derived macrophages (BMDMs) were obtained as previously described [28]. Following CO_2 euthanasia, femurs and tibias were collected, and bone marrow cells were flushed out with ice-cold PBS. The cell suspension was filtered, pelleted by centrifugation, and resuspended in RPMI-1640 medium supplemented with 10% FBS and 1% penicillin-streptomycin. For macrophage differentiation, cells were cultured for 7 days in medium containing 20% L929-conditioned medium (as a source of M-CSF). Adherent differentiated cells were defined as BMDMs and used for subsequent experiments.

RNA sequencing

Primary PMs isolated from *Sema7a*$^{-/-}$ and *Sema7a*$^{+/+}$ mice were treated with ox-LDL for 48 h (n = 3 per group). Total RNA was extracted via TRIzol reagent (DP419, TIANGEN) according to the manufacturer's instructions. RNA sequencing (RNA-seq) was conducted by Suzhou GENTLEGEN Biotechnology Co., Ltd. Briefly, sequencing was performed on an Illumina NovaSeq 6000 platform (paired-end). The raw reads were processed by trimming adapters and low-quality bases via TrimGalore, and the clean reads were aligned to the GRCm38/mm10 mouse reference genome with HISAT2. DAVID was utilized for Gene Ontology (GO) and Kyoto Encyclopedia of Genes and Genomes (KEGG) enrichment analysis, and the outcomes were graphically represented using ggplot2 in R.

Flow cytometry

PMs were stimulated for M1 polarization with 100 ng/mL IFN-γ + 100 ng/mL LPS for 24 h, followed by treatment with 10 μg/mL Dil-oxLDL (YB-0010, Yiyuanbiotech, China) for 48 h. After treatment, the cells were collected, washed three times with PBS, and analyzed via flow cytometry.

Immunoblotting

PMs and THP-1 cells were lysed in RIPA buffer (P0013B, Beyotime) supplemented with a protease and phosphatase inhibitor cocktail (5872, CST) and 1 mmol/L PMSF. Protein samples (30 μg) were heated to 100 °C for 10 min in sample buffer (LT101, EpiZyme). After blocking with 5% nonfat milk (D8340, Solarbio), membranes were washed with TBST and subsequently incubated with the following primary antibodies: mouse anti-human SEMA7A (1:1000, sc-374432, Santa Cruz), rabbit anti-human integrin β1 (1:2000, 12594-1-AP, Proteintech), sheep anti-mouse PLXNC1 (1:1000,

AF5375, RD Systems), goat anti-mouse MSR1 (0.2 μg/mL, AF1797, RD Systems), rabbit anti-human CD36 (1:1000, ab252923, Abcam), rabbit anti-mouse AKT (pan) (1:1000, 4691S, CST), rabbit anti-mouse Phospho-Akt (Ser473) (1:1000, 4060S, CST), rabbit anti-mouse Phospho-Akt (Thr308) (1:1000, 9275S, CST), mouse anti-mouse Phospho-SAPK/JNK (Thr183/Tyr185) (1:1000, 9255S, CST), rabbit anti-mouse SAPK/JNK (1:1000, 9252S, CST), rabbit anti-mouse p44/42 MAPK (Erk1/2) (1:1000, 4695T, CST), rabbit anti-mouse Phospho-p44/42 MAPK (Erk1/2) (Thr202/Tyr204) (1:1000, 4370T, CST), rabbit anti-mouse Tubulin (1:1000, AF1216, Beyotime), and mouse anti-mouse β-actin (1:1000, AF0003, Beyotime). After incubation at 4 °C overnight, the membranes were incubated with the following secondary antibodies: donkey anti-goat IRDye 800CW (1:10 000, 925–32214, LI-COR), rabbit anti-sheep IgG (H + L) cross-adsorbed secondary antibody (DyLight™ 800) (1:10 000, SA5-10060, Invitrogen), anti-rabbit IgG (H + L) (DyLight 800 4X PEG Conjugate) (1:10 000, 5151S, CST), and anti-mouse IgG (H + L) (DyLight 800 4X PEG Conjugate) (1:10 000, 5257S, CST). Proteins were detected with an Odyssey infrared imaging system (LI-COR, USA).

Immunofluorescence

Frozen sections (8 μm thick) were prepared using a Leica CM1950 cryostat (Leica Microsystems). The sections were incubated with the following primary antibodies: α-smooth muscle-Cy3™ (1:500, C6198, Sigma-Aldrich), rat anti-mouse CD11b (1:100, ab8878, Abcam), rabbit anti-mouse CD68 (1:100, 360018, Zenbio), rat anti-mouse CD31 (1:200, 557355, BD Biosciences), mouse anti-mouse SEMA7A (1:100, sc-374432, Santa Cruz), and rabbit anti-mouse MSR1 (1:100, ER1913-21, HUABIO). The secondary antibodies used included goat anti-rabbit IgG H&L Alexa Fluor® 647 (1:500, ab150079, Abcam), goat anti-mouse IgG H&L Alexa Fluor® 568 (1:500, ab175473, Abcam), and goat anti-rat IgG H&L Alexa Fluor® 488 (1:500, ab150165, Abcam). The sections were then mounted with DAPI Fluoromount-G (0100–20, SouthernBiotech), dried at room temperature overnight, and imaged via a confocal microscope (FV3000, Olympus).

Transcriptional analyses

Total RNA was isolated from PMs, BMDMs, and THP-1 cells using the RNA Extraction Kit (DP419, TIANGEN) following the manufacturer's protocol. The RNA was then reverse-transcribed using 5× All-in-one RT MasterMix (G490, abm). Quantitative reverse transcription-polymerase chain reaction (qRT-PCR) was conducted with LightCycler 480 SYBR Green I Master Mix (4887352001, Roche) on a LightCycler 480 II (Roche, Switzerland). *GAPDH* served as the internal reference gene. Primer sequences for qRT-PCR are provided in Table S1.

Statistical analysis

Statistical analyses were conducted via Prism 8.0 (GraphPad Prism Software). An unpaired two-tailed Student's *t*-test and one-way ANOVA were used to compare differences between groups, with statistical significance defined as $*P < 0.05$, $**P < 0.01$, $***P < 0.001$, and $****P < 0.0001$. The data are presented as the mean ± standard error of the mean (SEM). Differentially expressed genes (DEGs) for RNA-seq analysis were identified via the Wald test, as implemented in the "DESeq2" package.

Results

Upregulation of SEMA7A and its receptor integrin β1 during monocyte-to-macrophage differentiation

To examine the expression of SEMA7A in monocytes/macrophages, we analyzed transcriptomic data from human mononuclear cells [30] and revealed that SEMA7A expression was significantly greater in macrophages than in monocytes (Fig. 1A). Consistently, the transcription patterns of two known receptors for SEMA7A, integrin β1 (ITGB1) [12], and plexinC1 [31], mirrored those of SEMA7A, both of which presented increased expression in macrophages (Fig. 1B and 1C). To examine the expression of SEMA7A during monocyte-to-macrophage differentiation, we induced the differentiation of monocytic THP-1 cells into macrophages via the classical phorbol 12-myristate 13-acetate (PMA) [32]. qRT-PCR and Western blot analyses revealed a significant increase in the levels of SEMA7A mRNA and protein in a time-dependent manner upon PMA stimulation (Figs. S1A, 1D and 1E). Similarly, the mRNA and protein levels of integrin β1 were elevated following PMA stimulation (Figs. S1B, 1D and 1F). However, while qRT-PCR revealed an increase in the transcript level of plexinC1 during monocyte-to-macrophage differentiation (Fig. S1C), no significant change in plexinC1 protein expression was observed (Fig. S1D). For the pathophysiological relevance, ox-LDL was used to induce monocyte-to-macrophage differentiation in THP-1 cells. The results showed that ox-LDL induced the expression of SEMA7A (Fig. 1G and 1H) and integrin β1 (Fig. 1G and 1I).

The regulation of foamy macrophage differentiation plays a pivotal role in the progression of atherosclerotic plaques. To investigate the expression of SEMA7A in macrophages, we fed $Ldlr^{-/-}$ mice a WD for 12 weeks to

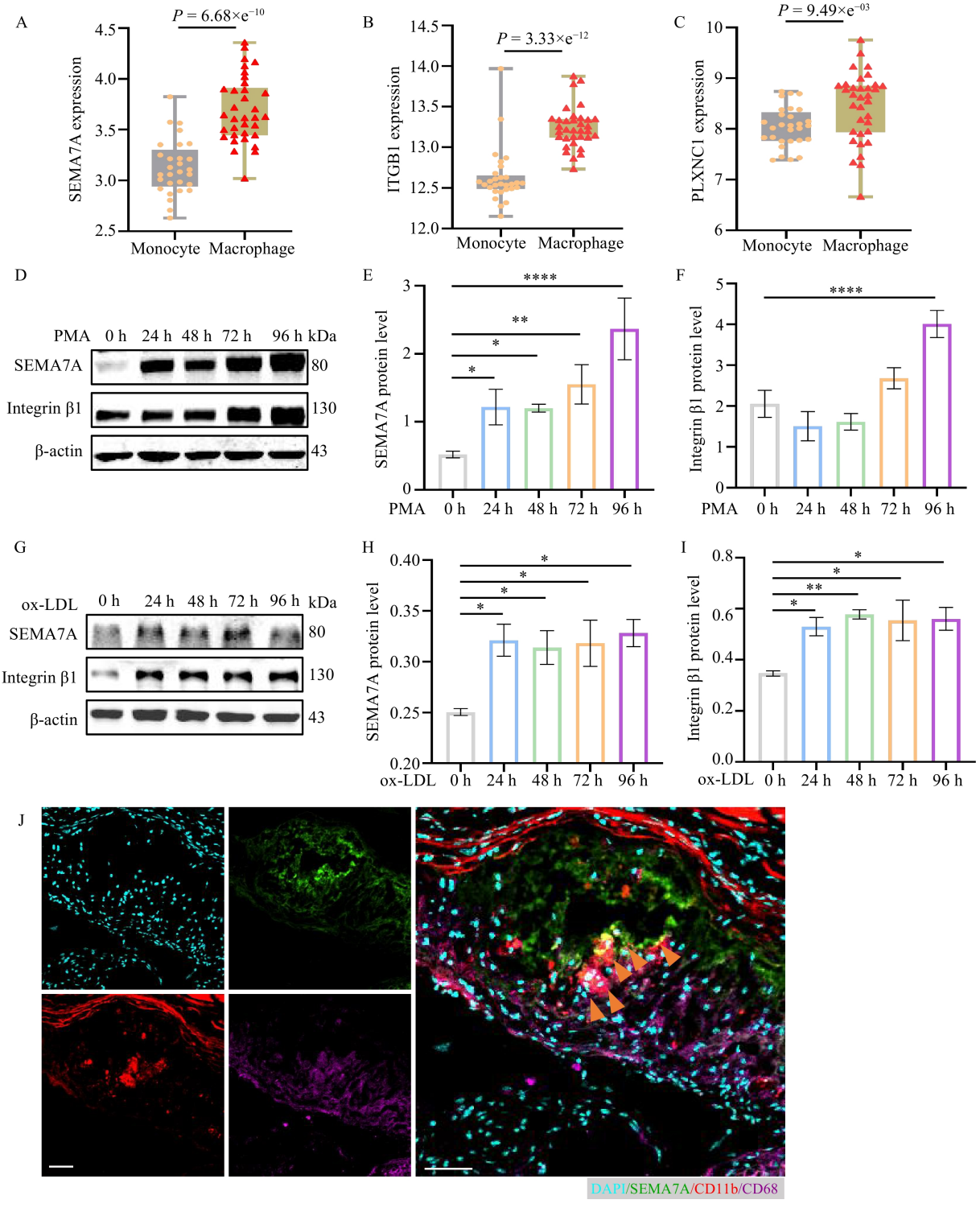

Fig. 1 Upregulation of SEMA7A and its receptor integrin β1 during monocyte-to-macrophage differentiation. (A–C) Expression levels of SEMA7A and its receptors in monocytes and macrophages derived from human mononuclear cells in the GEO database (Accession number: GSE9820). (D–F) Western blot analysis showing the protein levels of SEMA7A or integrin β1 at various time points in PMA-treated THP-1 cells. (G–I) Western blot analysis showing the protein levels of SEMA7A or integrin β1 at various time points in ox-LDL-treated THP-1 cells. (J) Representative immunofluorescence images showing the expression of SEMA7A, CD11b and CD68 in atherosclerotic plaques of *Ldlr*$^{-/-}$ mice. DAPI, cyan; SEMA7A, green; CD11b, red; CD68, magenta. Scale bar = 50 μm. Data are presented as the mean ± SEM, *$P < 0.05$, **$P < 0.01$, ***$P < 0.001$, ****$P < 0.0001$, one-way ANOVA.

induce atherosclerosis. Immunofluorescence staining demonstrated that SEMA7A was predominantly colocalized with $CD11b^+/CD68^+$ macrophages (Fig. 1J), with only limited overlap observed with $CD31^+$ endothelial cells within the atherosclerotic plaques (Fig. S1E), suggesting that SEMA7A is mainly expressed in plaque-associated macrophages. Collectively, these findings demonstrate that both SEMA7A and its receptor integrin β1 are upregulated during monocyte-to-macrophage differentiation and that SEMA7A is present in foamy macrophages within atherosclerotic lesions.

Macrophage SEMA7A deficiency reduces atherosclerotic lesions in the aortas of *Ldlr*$^{-/-}$ mice

To investigate the role of macrophage-derived SEMA7A in atherosclerosis, macrophage-specific *Sema7a* knockout mice were crossed with *Ldlr*$^{-/-}$ mice to generate *Sema7a*$^{\Delta M\phi}$ *Ldlr*$^{-/-}$ mice (Fig. S2A). After 12 weeks of WD feeding to induce atherosclerosis, the mice were sacrificed, and the whole aortas were stained with Sudan IV to assess plaque burden. As shown in Fig. 2A, the atherosclerotic lesion size in *Sema7a*$^{\Delta M\phi}$ *Ldlr*$^{-/-}$ mice was significantly reduced by 57.2% compared with that in *Sema7a*$^{fl/fl}$ *Ldlr*$^{-/-}$ mice ((16.3 ± 2.7)% of the total aorta area vs. (7.0 ± 0.4)% of the total aorta area, $P < 0.01$). Histological analysis of the aortic roots revealed that the lesion area in *Sema7a*$^{\Delta M\phi}$ *Ldlr*$^{-/-}$ mice was 58% smaller than that in *Sema7a*$^{fl/fl}$ *Ldlr*$^{-/-}$ mice ((29.5 ± 3.8)% vs. (12.4 ± 1.1)%, $P < 0.001$) (Fig. 2B). Oil red O staining of aortic root cross-sections revealed a 40.5% reduction in lipid deposition in *Sema7a*$^{\Delta M\phi}$ *Ldlr*$^{-/-}$ mice compared with *Sema7a*$^{fl/fl}$ *Ldlr*$^{-/-}$ mice ((35.9 ± 4.8)% vs. (21.4 ± 3.6)%, $P < 0.05$) (Fig. 2C). Additionally, body weight (Fig. S2B and S2C) and plasma lipid profiles (Fig. S2D–S2G) were comparable between *Sema7a*$^{\Delta M\phi}$ *Ldlr*$^{-/-}$ and *Sema7a*$^{fl/fl}$ *Ldlr*$^{-/-}$ mice.

To assess the impact of macrophage-derived SEMA7A on plaque stability, we evaluated the collagen content and the relative proportions of macrophages and smooth muscle cells in the aortic roots via Masson's trichrome staining and immunofluorescence staining. The collagen content within aortic root plaques was not significantly different between *Sema7a*$^{\Delta M\phi}$ *Ldlr*$^{-/-}$ and *Sema7a*$^{fl/fl}$ *Ldlr*$^{-/-}$ mice (Fig. 2D). However, the infiltration of MOMA2-positive macrophages increased in the aortic roots of macrophage-specific SEMA7A-deficient mice (Fig. 2E), whereas the smooth muscle cell content remained unchanged (Fig. 2F). To evaluate plaque stability, a "vulnerability index" was calculated via the formula: ((macrophage content (%) + lipid content (%)) / (smooth muscle cell content (%) + collagen content (%)). The results revealed that macrophage-derived SEMA7A deficiency significantly reduced the vulnerability index, suggesting an enhanced plaque stability (Fig. 2G). Taken together, these findings demonstrate that macrophage-derived SEMA7A promotes atherosclerosis progression and destabilizes plaques.

SEMA7A deficiency reduces the expression of MSR1 and lipid uptake in macrophages

To investigate the mechanism by which macrophage-derived SEMA7A promotes atherosclerosis progression, we first assessed the role of SEMA7A in lipid uptake. Primary *Sema7a*$^{-/-}$ and *Sema7a*$^{+/+}$ PMs were isolated and incubated with ox-LDL for 48 h. Oil red O and hematoxylin staining revealed that *Sema7a* deletion significantly reduced lipid accumulation by PMs (Fig. 3A). Consistently, flow cytometry analysis revealed a reduction in DiI-labeled ox-LDL uptake in SEMA7A-deficient PMs compared with that in *Sema7a*$^{+/+}$ PMs (Fig. 3B). Since CD36 and MSR1 are the key regulators of lipid uptake in macrophages, we examined their expression levels in SEMA7A-deficient PMs following ox-LDL stimulation. qRT-PCR analysis revealed that MSR1 transcription was reduced in both BMDMs and PMs from SEMA7A-deficient mice, whereas CD36 expression was downregulated only in PMs and remained unchanged in BMDMs (Fig. 3C–3F). Notably, the deletion of *Sema7a* had no observable impact on the expression levels of key cholesterol efflux-related genes, including *ABCA1*, *ABCG1*, and *SRB1* (Fig. S3), suggesting that SEMA7A specifically promotes lipid accumulation by enhancing uptake rather than impairing efflux. Further Western blot analysis revealed that *Sema7a* deletion reduced MSR1 protein expression, whereas CD36 expression remained unaffected (Fig. 3G–3I). Immunofluorescence analysis also revealed a reduction in MSR1 expression following *Sema7a* deletion (Fig. 3J). These findings indicate that SEMA7A deficiency downregulates MSR1 expression and reduces lipid uptake in macrophages.

JNK signaling pathway mediates MSR1 expression and lipid uptake in macrophages by SEMA7A

To elucidate the molecular mechanism by which macrophage-derived SEMA7A regulates lipid uptake, RNA-seq was performed on *Sema7a*$^{+/+}$ and *Sema7a*$^{-/-}$ PMs following ox-LDL stimulation. A total of 254 DEGs were identified, including 114 upregulated genes and 110 downregulated genes, in *Sema7a*$^{-/-}$ PMs compared with *Sema7a*$^{+/+}$ PMs (Fig. 4A). A heatmap of the top 10 most significantly altered DEGs is shown in Fig. S4. Subsequently, KEGG pathway analysis of the DEGs revealed the top five enriched signaling pathways, including viral protein interaction with cytokine and cytokine receptor, the MAPK signaling pathway, cellular senescence, cytokine-cytokine receptor interaction, and

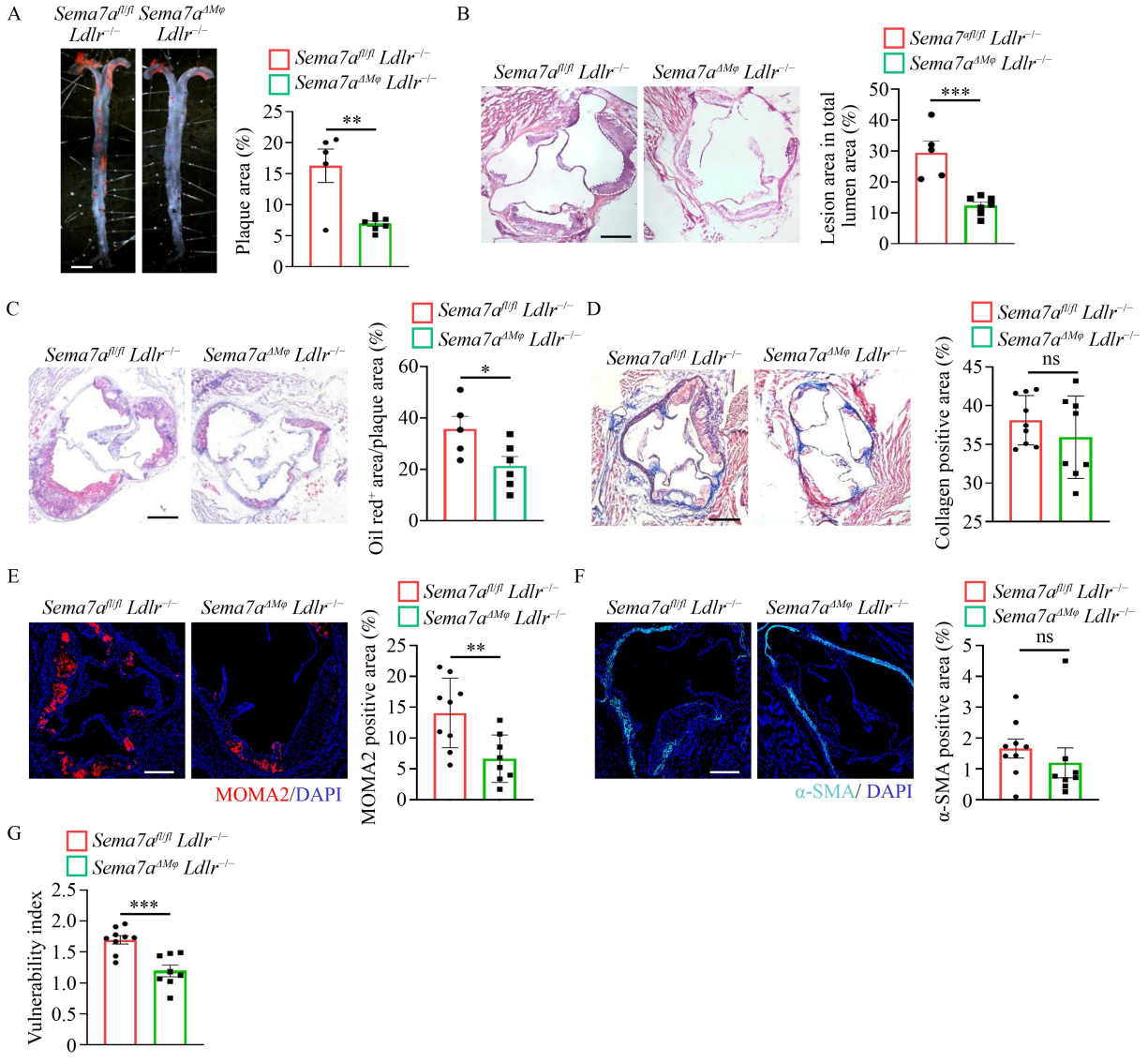

Fig. 2 Macrophage-specific SEMA7A deficiency reduces atherosclerotic lesions in the aorta of *Ldlr*$^{-/-}$ mice. (A) Sudan IV staining and quantitative analysis of total aorta from *Sema7a*$^{\Delta M\phi}$ *Ldlr*$^{-/-}$ and *Sema7a*$^{fl/fl}$ *Ldlr*$^{-/-}$ mice after 12 weeks on WD. $N \geqslant 5$. Scale bar = 2 mm. (B) HE staining of aortic root sections from *Sema7a*$^{\Delta M\phi}$ *Ldlr*$^{-/-}$ and *Sema7a*$^{fl/fl}$ *Ldlr*$^{-/-}$ mice after 12 weeks on WD. $N \geqslant 5$. Scale bar = 200 μm. (C) Oil red O staining of aortic root sections from *Sema7a*$^{\Delta M\phi}$ *Ldlr*$^{-/-}$ and *Sema7a*$^{fl/fl}$ *Ldlr*$^{-/-}$ mice after 12 weeks on WD. $N \geqslant 5$. Scale bar = 200 μm. (D) Masson's trichrome staining of aortic root sections from *Sema7a*$^{\Delta M\phi}$ *Ldlr*$^{-/-}$ and *Sema7a*$^{fl/fl}$ *Ldlr*$^{-/-}$ mice after 12 weeks on WD. $N \geqslant 8$. Scale bar = 200 μm. (E) Representative immunofluorescence images showing macrophages in the aortic root of *Sema7a*$^{\Delta M\phi}$ *Ldlr*$^{-/-}$ and *Sema7a*$^{fl/fl}$ *Ldlr*$^{-/-}$ mice after 12 weeks of WD. MOMA2, red; DAPI, blue. $N \geqslant 8$. Scale bar = 200 μm. (F) Representative immunofluorescence images showing vascular smooth muscle cells in the aortic root of *Sema7a*$^{\Delta M\phi}$ *Ldlr*$^{-/-}$ and *Sema7a*$^{fl/fl}$ *Ldlr*$^{-/-}$ mice after 12 weeks on WD. α-SMA, cyan; DAPI, blue. $N \geqslant 8$. (G) Vulnerability index of atherosclerotic plaques in the aortic root of *Sema7a*$^{\Delta M\phi}$ *Ldlr*$^{-/-}$ and *Sema7a*$^{fl/fl}$ *Ldlr*$^{-/-}$ mice after 12 weeks of WD. $N \geqslant 8$. Data are presented as the mean ± SEM, $^{*}P < 0.05$, $^{**}P < 0.01$, $^{***}P < 0.001$, Student's *t*-test.

platelet activation (Fig. 4B). Notably, the MAPK signaling pathway contained the highest proportion of DEGs among all enriched pathways, prompting us to investigate its role in SEMA7A-mediated lipid uptake. Western blot analysis revealed that phosphorylation of JNK was significantly reduced in PMs isolated from SEMA7A-deficient mice after ox-LDL stimulation, whereas ERK phosphorylation remained unchanged (Fig. 4C and 4D), suggesting that the JNK signaling pathway is involved in the role of SEMA7A in lipid uptake by macrophages.

The role of the JNK signaling pathway in mediating lipid uptake by SEMA7A was further investigated via pharmacological approaches. Western blot and qRT-PCR analysis revealed that 20 μmol/L SP600125 sufficiently inhibited phosphorylation of JNK and MSR1 expression (Figs. 4E and S5). Immunofluorescence staining showed that 20 μmol/L SP600125 effectively suppressed MSR1

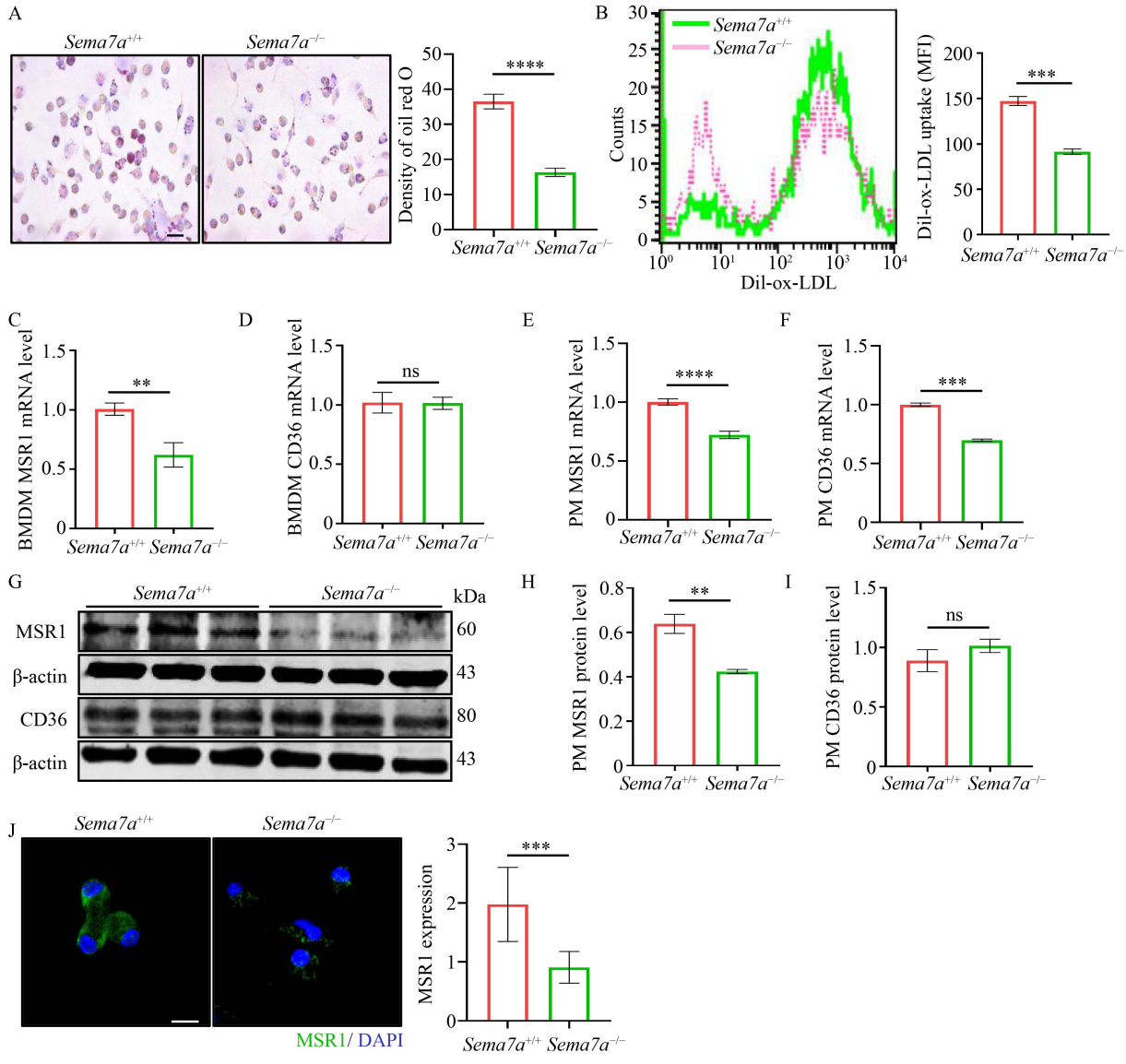

Fig. 3 SEMA7A deficiency reduces the expression of MSR1 and lipid uptake in macrophages. (A) Oil red O and hematoxylin staining showing the lipid accumulation in *Sema7a*$^{-/-}$ and *Sema7a*$^{+/+}$ PMs after incubated with ox-LDL for 48 h. Scale bar = 20 μm. (B) Flow cytometry analysis showing the lipid uptake in *Sema7a*$^{-/-}$ and *Sema7a*$^{+/+}$ PMs after incubated with 10 μg/mL Dil-ox-LDL for 48 h. (C–F) qRT-PCR analysis of MSR1 and CD36 expression in BMDM and PMs after incubation with ox-LDL for 48 h. (G–I) Western blot analysis of MSR1 and CD36 protein levels in *Sema7a*$^{-/-}$ and *Sema7a*$^{+/+}$ PMs after incubated with ox-LDL for 48 h. (J) Representative immunofluorescence images and quantification of MSR1 expression in *Sema7a*$^{-/-}$ and *Sema7a*$^{+/+}$ PMs after incubated with ox-LDL for 48 h. Scale bar = 10 μm. Data are presented as the mean ± SEM, $^{**}P < 0.01$, $^{***}P < 0.001$, $^{****}P < 0.0001$, Student's *t*-test.

expression in *Sema7a*$^{+/+}$ PMs but not in *Sema7a*$^{-/-}$ PMs (Fig. 4F). Importantly, JNK inhibitor SP600125 significantly reduced lipid deposition in ox-LDL-stimulated *Sema7a*$^{+/+}$ PMs, even in *Sema7a*$^{-/-}$ PMs, as shown by the density of Oil red O-positive areas (Fig. 4G). Consistently, flow cytometry analysis showed that treatment of ox-LDL-stimulated PMs with a JNK inhibitor significantly reduced the mean fluorescence intensity (MFI) of macrophages after incubation with DiI-labeled ox-LDL in *Sema7a*$^{+/+}$ PMs or in *Sema7a*$^{-/-}$ PMs (Fig. 4H and 4I). These findings indicate that SEMA7A promotes lipid uptake in macrophages, likely by regulating MSR1 expression through the JNK signaling pathway.

SEMA7A promotes macrophage lipid uptake through the integrin β1-mediated JNK/MSR1 axis

Given the observed upregulation of integrin β1 in ox-LDL-stimulated monocytic THP-1 cells, we hypothesized that integrin β1, a key receptor for SEMA7A, might play a pivotal role in SEMA7A signaling in macrophages. To

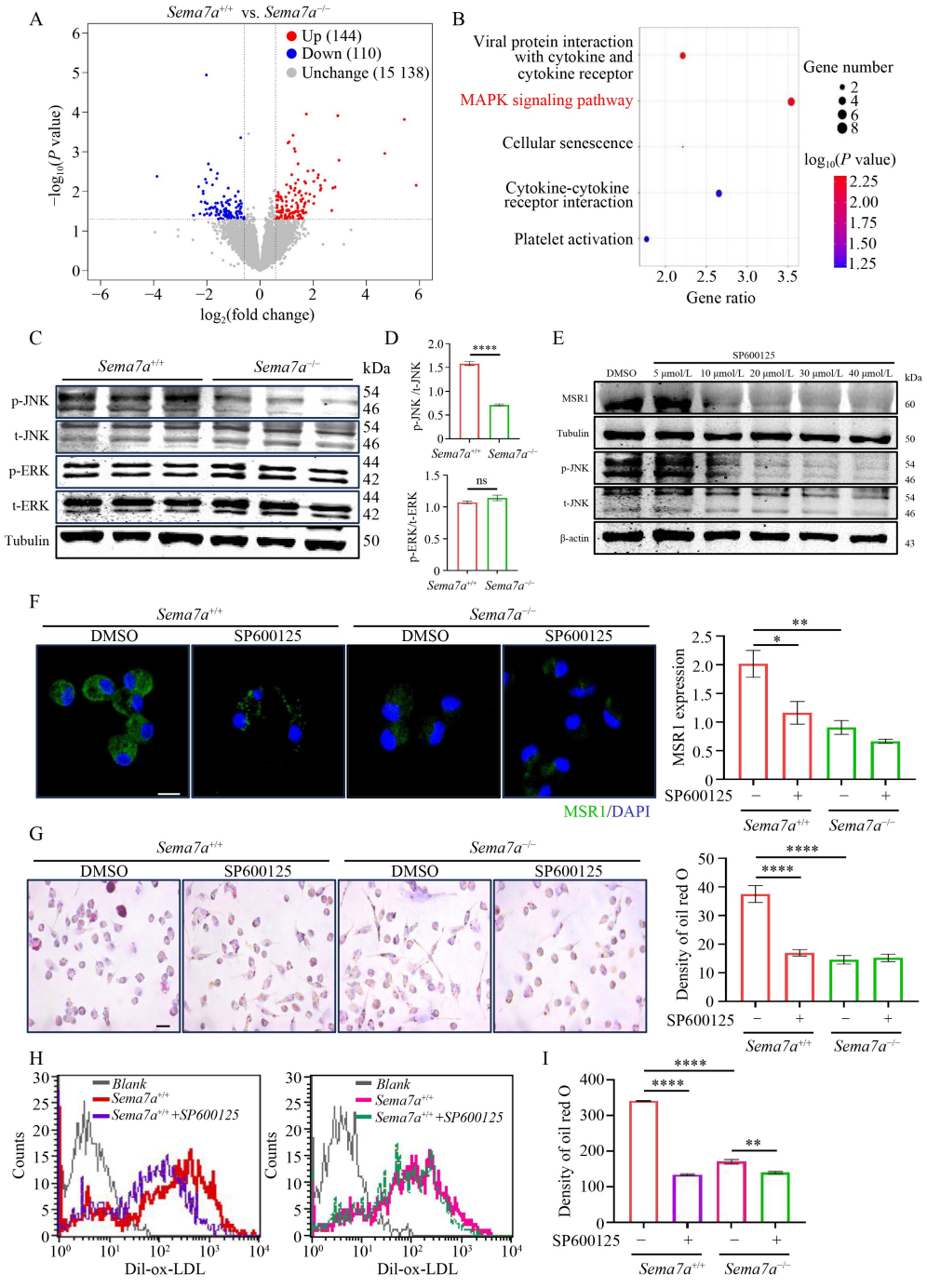

Fig. 4 The JNK signaling pathway mediates MSR1 expression and lipid uptake in macrophages via SEMA7A. (A) Volcano plot displaying the DEGs of PMs isolated from *Sema7a*$^{+/+}$ and *Sema7a*$^{-/-}$ mice after ox-LDL stimulation. The DEGs from RNA-seq analysis were identified using the Wald test. (B) Bubble plot depicting the top 5 enriched KEGG pathways in the DEGs. (C, D) Western blot analysis of phosphorylated and total JNK (p-JNK, t-JNK), and ERK (p-ERK, t-ERK) protein levels in PMs isolated from *Sema7a*$^{+/+}$ and *Sema7a*$^{-/-}$ mice after ox-LDL stimulation. Data are presented as the mean ± SEM, ****$P < 0.0001$, Student's *t*-test. (E) Western blot analysis of phosphorylated and total JNK (p-JNK, t-JNK) and MSR1 protein levels in PMs isolated from *Sema7a*$^{+/+}$ mice after incubation with ox-LDL and various concentrations of SP600125 for 48 h. (F) Representative immunofluorescence images and statistical analyses of MSR1 expression in the *Sema7a*$^{-/-}$ and *Sema7a*$^{+/+}$ PMs after incubated with ox-LDL and SP600125 for 48 h. Data are presented as the mean ± SEM, *$P < 0.05$, **$P < 0.01$, one way ANOVA. MSR1, green; DAPI, blue. Scale bar = 10 μm. (G) Oil red O and hematoxylin staining showing lipid accumulation in *Sema7a*$^{-/-}$ and *Sema7a*$^{+/+}$ PMs after incubated with ox-LDL and the 20 μmol/L JNK inhibitor SP600125 for 48 h. Data are presented as the mean ± SEM, ****$P < 0.0001$, one-way ANOVA. Scale bar = 20 μm. (H, I) Flow cytometry analysis showing the lipid uptake in *Sema7a*$^{+/+}$ and *Sema7a*$^{-/-}$ PMs after incubated with Dil-oxLDL and SP600125 for 48 h. Data are presented as the mean ± SEM, *$P < 0.05$, **$P < 0.01$, ****$P < 0.0001$, one-way ANOVA.

test this hypothesis, we employed the integrin β1 inhibitor GLPG0187 [33] to block SEMA7A-evoked signaling in macrophages. We first examined the effective dose of GLPG0187 for inhibition and showed that 40 nmol/L GLPG0187 sufficiently inhibited JNK phosphorylation and MSR1 expression in PMs upon ox-LDL incubation (Fig. 5A–5C). We then used 40 nmol/L GLPG0187 to treat PMs and found that GLPG0187 significantly reduced p-JNK levels (Fig. 5D and 5E) and MSR1 expression (Fig. 5D and 5F) in *Sema7a*$^{+/+}$ PMs, even to the level in *Sema7a*$^{-/-}$ PMs (Fig. 5D and 5F). Moreover, GLPG0187 effectively inhibited lipid uptake in ox-LDL-stimulated *Sema7a*$^{+/+}$ PMs, as shown by the density of the Oil red O-positive areas, even the level in *Sema7a*$^{-/-}$ PMs (Fig. 5G). Consistently, immunofluorescence staining showed that GLPG0187 significantly suppressed

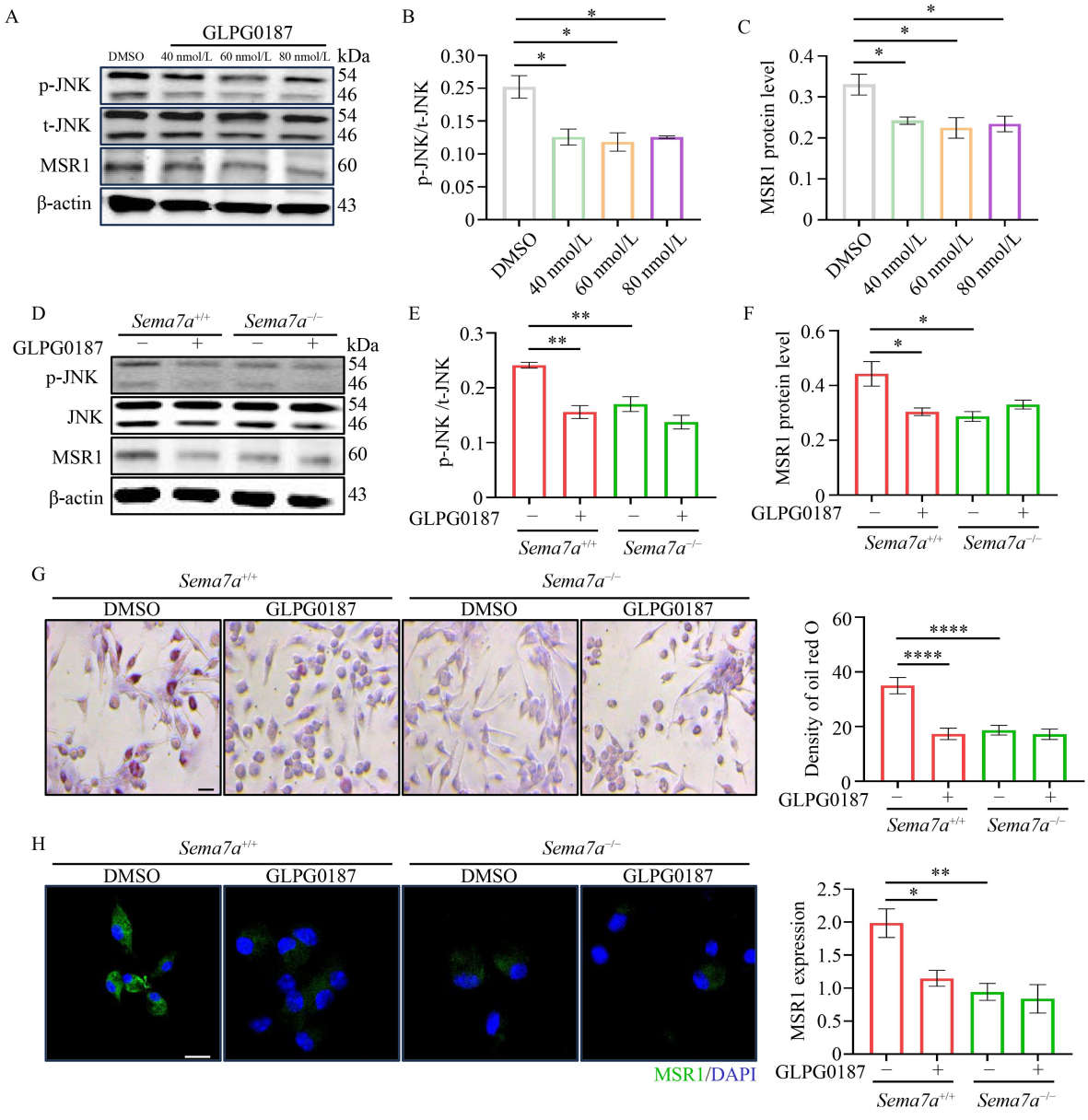

Fig. 5 SEMA7A regulates macrophage lipid uptake through the integrin β1-mediated JNK/MSR1 axis. (A–C) Western blot analysis of phosphorylated and total JNK (p-JNK, t-JNK), and MSR1 protein levels in *Sema7a*$^{+/+}$ PMs after incubation with ox-LDL and various concentrations of integrin β1 inhibitor GLPG0187 for 48 h. (D–F) Western blot analysis of phosphorylated and total JNK (p-JNK, t-JNK), and MSR1 protein levels in *Sema7a*$^{-/-}$ and *Sema7a*$^{+/+}$ PMs after incubation with ox-LDL and 40 nmol/L GLPG0187 for 48 h. (G) Oil red O and hematoxylin staining showing lipid accumulation in *Sema7a*$^{-/-}$ and *Sema7a*$^{+/+}$ PMs after incubation with ox-LDL and GLPG0187 (40 nmol/L) for 48 h. Scale bar = 20 μm. (H) Representative immunofluorescence images and statistical analyses of MSR1 expression in *Sema7a*$^{-/-}$ and *Sema7a*$^{+/+}$ PMs after incubation with ox-LDL and GLPG0187 for 48 h. MSR1, green; DAPI, blue. Data are presented as the mean ± SEM, $*P < 0.05$, $**P < 0.01$, $****P < 0.0001$, one-way ANOVA. Scale bar = 10 μm.

MSR1 expression in *Sema7a*$^{+/+}$ PMs, even in *Sema7a*$^{-/-}$ PMs (Fig. 5H). Together, these findings suggest that integrin β1 plays a critical role in mediating SEMA7A-promoted macrophage lipid uptake via the JNK/MSR1 axis.

Administration of GLPG0187 attenuates the progression of carotid atherosclerotic plaques

On the basis of the key role of GLPG0187 in regulating macrophage lipid uptake and considering the lack of evidence demonstrating its direct involvement in atherosclerosis progression, we next evaluated the potential therapeutic effects of GLPG0187 on atherosclerosis development. We established a mouse carotid atherosclerosis model by intravenously injecting AAV-mPCSK9^{DY} after partial carotid artery ligation [28] (Fig. 6A). Ten-week-old male mice received an intravenous injection of 2 mg/kg GLPG0187 one day before carotid atherosclerosis was induced. During the two weeks of WD feeding following model establishment, the mice were administered intravenous injections of GLPG0187 every other day. Notably, treatment with GLPG0187 resulted in a significant reduction in atherosclerotic lesion size compared with that in the control group ((40.0 ± 7.3)% vs. (14.6 ± 4.4)%, $P < 0.01$) (Fig. 6B). Histological analysis showed that the lesion area in the carotid artery was reduced by 79.5% in the GLPG0187-treated group compared with the DMSO group (Fig. 6C). Notably, Oil red O staining revealed a 69.2% reduction in lipid deposition within carotid artery plaques in the GLPG0187-treated group compared with the DMSO group (Fig. 6D). Together, these findings indicate that the inhibition of integrin β1 by GLPG0187 attenuates the progression of carotid atherosclerotic plaques.

Discussion

In this study, we demonstrated that SEMA7A expression is upregulated during the differentiation of monocytes into macrophages and that macrophage-specific *Sema7a* deletion attenuated atherosclerosis progression and enhanced plaque stability in *Ldlr*$^{-/-}$ mice. Mechanistically, SEMA7A promoted macrophage lipid uptake via the integrin β1-mediated JNK/MSR1 signaling pathway. Notably, pharmacological inhibition of integrin β1 with GLPG0187 effectively suppressed atherosclerosis progression. To our knowledge, this is the first report demonstrating that SEMA7A facilitates atherosclerosis development through regulation of macrophage lipid uptake, offering new insights into potential therapeutic interventions.

SEMA7A, which is expressed by a variety of cell types including red blood cells, T cells, macrophages, and endothelial cells, has emerged as a critical mediator in

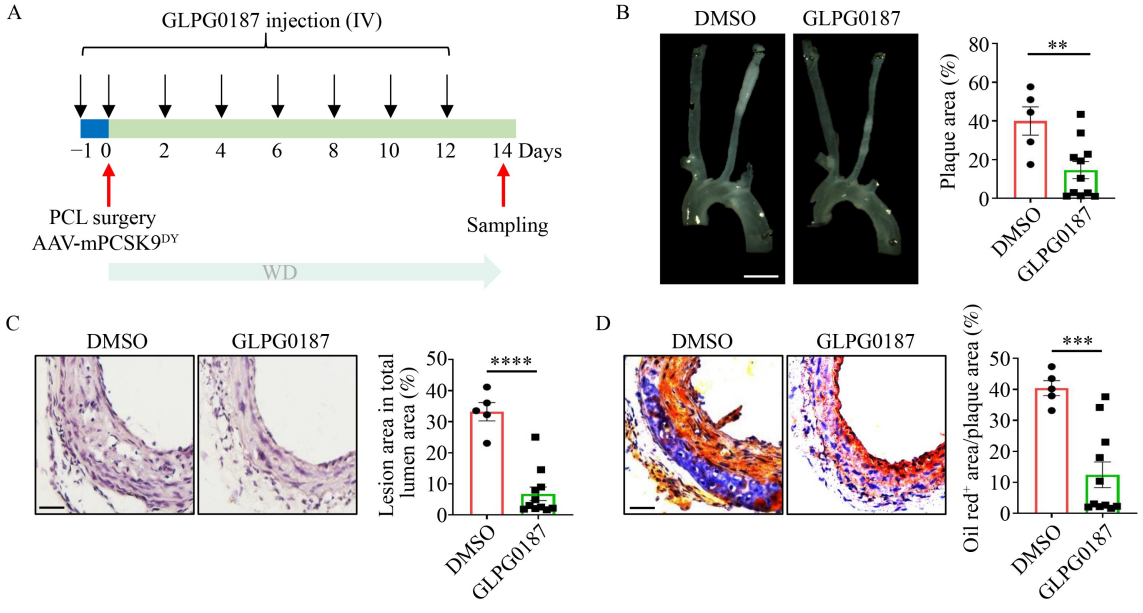

Fig. 6 Administration of GLPG0187 attenuates the progression of carotid atherosclerotic plaques. (A) Schematic diagram illustrating the experimental design for evaluating the effects of GLPG0187 administration in a mouse carotid atherosclerosis model. GLPG0187 dissolved in DMSO, then further dissolved in a solution containing 65% ddH_2O, 30% PEG300, and 5% Tween 80. (B) Representative stereo microscopic images of aortas from mice treated with GLPG0187 following carotid atherosclerosis induction. $N \geq 5$. Scale bar = 1 mm. (C) HE staining of carotid atherosclerotic plaques from mice treated with DMSO or GLPG0187. $N \geq 5$. Scale bar = 20 μm. Data are presented as the mean ± SEM, ****$P < 0.0001$, Student's *t*-test. (D) Oil red O staining of carotid atherosclerotic plaques from mice treated with DMSO or GLPG0187. $N \geq 5$. Scale bar = 20 μm. Data are presented as the mean ± SEM, **$P < 0.01$, ***$P < 0.001$, Student's *t*-test.

multiple inflammation-related diseases. In macrophages, SEMA7A has been shown to promote macrophage differentiation and polarization toward the pro-resolving M2 phenotype [34] and to function as an inflammation regulator in Coxsackievirus B3 (CVB3)-induced viral myocarditis [35]. Despite the established involvement of SEMA7A in various inflammatory conditions, the precise function of macrophage-derived SEMA7A in the context of atherosclerosis has yet to be elucidated. This gap in knowledge highlights the need for focused studies to uncover how SEMA7A produced by macrophages influences plaque development and progression. In this study, we demonstrated that macrophage-derived SEMA7A deficiency attenuates atherosclerosis progression and enhances the stability of atherosclerotic plaques. SEMA7A promotes lipid uptake by upregulating MSR1 expression. This finding fills a gap in our understanding of SEMA7A in atherosclerosis, as we recently proposed that endothelial Sema7A plays a critical role in atherosclerosis in response to disturbed flow [20]. Notably, in our previous investigation on the role of SEMA7A in the development of atherosclerosis, bone marrow transplantation experiments implied that vascular-derived SEMA7A contributes more significantly to plaque formation than does hematopoietic SEMA7A [20]. However, the observations from these two studies are not inconsistent, as the previous notion could not exclude the role of hematopoietic SEMA7A in atherosclerosis. Moreover, different conditions need to be considered when interpreting the data between these two observations, such as the genetic background of the *Apoe*$^{-/-}$ and *Ldlr*$^{-/-}$ mouse models and the procedures used to induce the atherosclerotic model, classical WD-induced plaque formation versus extended-PCL + WD-induced plaque formation.

The biological functions of SEMA7A are primarily mediated through two well-characterized receptors: integrin β1 (ITGB1) and plexinC1 (PLXNC1) [36]. During monocyte-to-macrophage differentiation, we observed that the expression of integrin β1 increased in parallel with the upregulation of SEMA7A, whereas plexinC1 expression remained unchanged, suggesting that integrin β1 may play a pivotal role in SEMA7A-mediated macrophage lipid uptake. Consistent with this hypothesis, treatment of macrophages with the integrin β1 inhibitor GLPG0187 significantly downregulated the expression of MSR1 and suppressed macrophage lipid uptake. Through the focal adhesion complex, integrin β1 may activate the MAPK signaling pathway or other downstream pathways. RNA-seq and pharmacological approaches have revealed that the MAPK/JNK signaling pathway is the major pathway that mediates the role of SEMA7A in promoting MSR1 expression and lipid uptake downstream of integrin β1 in macrophages. However, we cannot exclude the role of the AKT signaling pathway in SEMA7A-induced lipid uptake. In fact, administration of the AKT inhibitor MK2206 significantly reduced lipid deposition in ox-LDL-stimulated PMs (Fig. S6A). Consistently, flow cytometry analysis revealed that treatment of ox-LDL-stimulated PMs with an AKT inhibitor significantly reduced the mean fluorescence intensity (MFI) of the macrophages (Fig. S6B). Furthermore, Western blot analysis showed that the phosphorylation of AKT was significantly lower in PMs isolated from SEMA7A-deficient mice than in those isolated from WT mice after ox-LDL stimulation (Fig. S6C–S6E), suggesting the involvement of the AKT signaling pathway in SEMA7A-mediated lipid uptake in macrophages. However, the AKT inhibitor MK2206 did not effectively downregulate MSR1 expression in ox-LDL-stimulated PMs (Fig. S6F and S6G). The mechanism by which AKT regulates SEMA7A-induced lipid uptake in macrophages deserves further investigation.

In this study, we utilized macrophage-specific *Sema7a* knockout mice to selectively examine the role of macrophage-derived SEMA7A in atherosclerosis. While our results support a dominant role for macrophage-derived SEMA7A in lipid uptake and atherosclerotic lesion progression, we are unable to fully exclude the influence of SEMA7A from other sources as SEMA7A can also be produced by other cell types such as endothelial cells, red blood cells, and lymphocytes, potentially influencing plaque development. In fact, our previous study indicates a role of vascular SEMA7A expression by disturbed blood flow in atherosclerosis [20]. Moreover, expression of SEMA7A by multiple cell types may contribute to the SEMA7A pool in the circulation, promoting atherosclerosis. Further investigations using other cell type-specific *Sema7a* knockout mice or an approach applying soluble SEMA7A in global *Sema7a* knockout mice will be necessary to fully delineate the systemic and cell-type specific contributions of SEMA7A in atherosclerosis.

GLPG0187 may represent a promising therapeutic candidate for the prevention and treatment of atherosclerosis. Given that GLPG0187 has demonstrated a favorable safety profile and is in phase I clinical trials for the treatment of solid tumors [37], we sought to investigate its effects on the progression of atherosclerotic plaques in a mouse carotid atherosclerosis model. Notably, our results demonstrated that the administration of GLPG0187 significantly attenuated the progression of carotid artery plaques, highlighting its potential as a novel therapeutic strategy for atherosclerosis. While our study primarily focused on the macrophage-related mechanisms, it is important to note that GLPG0187 is a broad-spectrum integrin antagonist that has been used to block αvβ6 integrin receptors on cancer cells [38] and to inhibit integrin β1 on human bronchial epithelial cells, thereby modulating asthma progression [33]. Given its

broad activity, GLPG0187 may also affect other integrin-dependent cellular processes, such as endothelial cell adhesion, vascular smooth muscle cell migration, and extracellular matrix remodeling. These effects could also contribute to the plaque formation. Therefore, future studies should aim to delineate the cell type-specific actions of GLPG0187 in the atherosclerotic microenvironment.

Conclusions

Our study identified macrophage-derived SEMA7A as a pivotal driver of atherosclerosis, promoting macrophage lipid uptake through activation of the JNK/MSR1 signaling axis via the integrin β1 receptor. Notably, pharmacological inhibition of integrin β1 with GLPG0187 effectively attenuated atherosclerosis progression, highlighting a promising strategy for the prevention and treatment of atherosclerosis.

Acknowledgements

This work was supported by the National Natural Science Foundation of China (Nos. 82170466, 82470483 to Li Zhu, 82070450 to Chaojun Tang), the Natural Science Foundation of Jiangsu Province (No. BK20230487 to Fengchan Li), the fellowship of China Postdoctoral Science Foundation (No. 7121102223 to Fengchan Li), and the Priority Academic Program Development of Jiangsu Higher Education Institutions of China (to Li Zhu).

Compliance with ethics guidelines

Conflicts of interest Fengchan Li, Haofu Ni, Fan Tang, Jiaxin Lyu, Lili Wu, Lijie Ren, Qiongyu Lu, Shouming Zhao, Chaojun Tang, and Li Zhu declare that they have no conflict of interest.

The study was conducted in accordance with the Declaration of Helsinki. All animal experiments were approved by the Ethics Committee of Soochow University and conducted under specific pathogen-free barrier conditions in accordance with the institutional guidelines of the Laboratory Animal Center of Soochow University.

Electronic supplementary material Supplementary material is available in the online version of this article at https://doi.org/10.1007/s11684-025-1181-z and is accessible for authorized users.

References

1. Zhao D, Liu J, Wang M, Zhang X, Zhou M. Epidemiology of cardiovascular disease in China: current features and implications. Nat Rev Cardiol 2019; 16(4): 203–212
2. Jimenez-Trinidad FR, Calvo-Gomez S, Sabate M, Brugaletta S, Campuzano V, Egea G, Dantas AP. Extracellular vesicles as mediators of endothelial dysfunction in cardiovascular diseases. Int J Mol Sci 2025; 26(3): 1008
3. Dong Z, Jin Y, Shen Y, Huang J, Tan J, Feng Q, Gong Z, Zhu S, Chen H, Yu F, Li W, Jia Y, Kong W, Fu Y. METTL3-catalyzed m6A methylation facilitates the contribution of vascular smooth muscle cells to atherosclerosis. Cardiovasc Res 2025; 121(4): 568–584
4. Xu S, Yang B, Yu W, Gao Y, Cai H, Wang Z. TREM2 as a therapeutic target in atherosclerosis. Cell Biol Int 2025; 49(4): 305–316
5. Fang F, Wang E, Fang M, Yue H, Yang H, Liu X. Macrophage-based pathogenesis and theranostics of vulnerable plaques. Theranostics 2025; 15(4): 1570–1588
6. Xiang X, Zhang F, Nie L, Guo X, Qin M, Chen J, Jiang D, Zhang Z, Mao L. Legumain deficiency halts atherogenesis by modulating T cell receptor signaling. Aging Cell 2025; 24(2): e14391
7. Guo Z, Zhang W, Gao H, Li Y, Li X, Yang X, Fan L. High expression levels of haem oxygenase-1 promote ferroptosis in macrophage-derived foam cells and exacerbate plaque instability. Redox Biol 2024; 76: 103345
8. Libby P, Ridker PM, Hansson GK. Progress and challenges in translating the biology of atherosclerosis. Nature 2011; 473(7347): 317–325
9. Li S, Navia-Pelaez JM, Choi SH, Miller YI. Macrophage inflammarafts in atherosclerosis. Curr Opin Lipidol 2023; 34(5): 189–195
10. Chen Y, Zhang J, Cui W, Silverstein RL. CD36, a signaling receptor and fatty acid transporter that regulates immune cell metabolism and fate. J Exp Med 2022; 219(6): e20211314
11. Liu Y, Tang X, Yuan H, Gao R. Naringin inhibits macrophage foam cell formation by regulating lipid homeostasis and metabolic phenotype. Nutrients 2024; 16(9): 1321
12. Pasterkamp RJ, Peschon JJ, Spriggs MK, Kolodkin AL. Semaphorin 7A promotes axon outgrowth through integrins and MAPKs. Nature 2003; 424(6947): 398–405
13. Pasterkamp RJ, Kolk SM, Hellemons AJ, Kolodkin AL. Expression patterns of semaphorin7A and plexinC1 during rat neural development suggest roles in axon guidance and neuronal migration. BMC Dev Biol 2007; 7(1): 98
14. Eixarch H, Gutierrez-Franco A, Montalban X, Espejo C. Semaphorins 3A and 7A: potential immune and neuroregenerative targets in multiple sclerosis. Trends Mol Med 2013; 19(3): 157–164
15. CantóE, Tintore M, Villar LM, Borras E, Alvarez-Cermeno JC, Chiva C, Sabido E, Rovira A, Montalban X, Comabella M. Validation of semaphorin 7A and ala-beta-his-dipeptidase as biomarkers associated with the conversion from clinically isolated syndrome to multiple sclerosis. J Neuroinflammation 2014; 11(1): 181
16. Tarullo SE, Hill RC, Hansen KC, Behbod F, Borges VF, Nelson AC, Lyons TR. Postpartum breast cancer progression is driven by semaphorin 7a-mediated invasion and survival. Oncogene 2020; 39(13): 2772–2785
17. Garcia-Areas R, Libreros S, Simoes M, Castro-Silva C, Gazaniga N, Amat S, Jaczewska J, Keating P, Schilling K, Brito M, Wojcikiewicz EP, Iragavarpu-Charyulu V. Suppression of tumor-derived Semaphorin 7A and genetic ablation of host-derived Semaphorin 7A impairs tumor progression in a murine model of

advanced breast carcinoma. Int J Oncol 2017; 51(5): 1395–1404
18. Granja T, Kohler D, Tang L, Burkard P, Eggstein C, Hemmen K, Heinze KG, Heck-Swain KL, Koeppen M, Gunther S, Blaha M, Magunia H, Bamberg M, Konrad F, Ngamsri KC, Fuhr A, Keller M, Bernard AM, Haeberle HA, Bakchoul T, Zarbock A, Nieswandt B, Rosenberger P. Semaphorin 7A coordinates neutrophil response during pulmonary inflammation and sepsis. Blood Adv 2024; 8(11): 2660–2674
19. Lu Q, Liu Z, Zhao L, Xu L, Liu C, Li L, Cao Y, Li F, Wu L, Wang L, Chen T, You T, Ren L, Wang G, Tang C, Zhu L. Sema7A protects against high-fat diet-induced obesity and hepatic steatosis by regulating adipo/lipogenesis. Mol Metab 2023; 70: 101698
20. Hu S, Liu Y, You T, Heath J, Xu L, Zheng X, Wang A, Wang Y, Li F, Yang F, Cao Y, Zhang H, van Gils JM, van Zonneveld AJ, Jo H, Wu Q, Zhang Y, Tang C, Zhu L. Vascular semaphorin 7A upregulation by disturbed flow promotes atherosclerosis through endothelial beta1 integrin. Arterioscler Thromb Vasc Biol 2018; 38(2): 335–343
21. Köhler D, Granja T, Volz J, Koeppen M, Langer HF, Hansmann G, Legchenko E, Geisler T, Bakchoul T, Eggstein C, Haberle HA, Nieswandt B, Rosenberger P. Red blood cell-derived semaphorin 7A promotes thrombo-inflammation in myocardial ischemia-reperfusion injury through platelet GPIb. Nat Commun 2020; 11(1): 1315
22. Hu S, Liu Y, You T, Zhu L. Semaphorin 7A promotes VEGFA/VEGFR2-mediated angiogenesis and intraplaque neovascularization in *ApoE*$^{-/-}$ mice. Front Physiol 2018; 9: 1718
23. Hong L, Li F, Tang C, Li L, Sun L, Li X, Zhu L. Semaphorin 7A promotes endothelial to mesenchymal transition through ATF3 mediated TGF-beta2/Smad signaling. Cell Death Dis 2020; 11(8): 695
24. Song X, Gao F, Li H, Qin W, Chai C, Shi G, Yang H. Semaphorin 7A promotes human vascular smooth muscle cell proliferation and migration through the β-catenin signaling pathway. Biocell 2023; 47(4): 849–858
25. Suzuki K, Okuno T, Yamamoto M, Pasterkamp RJ, Takegahara N, Takamatsu H, Kitao T, Takagi J, Rennert PD, Kolodkin AL, Kumanogoh A, Kikutani H. Semaphorin 7A initiates T-cell-mediated inflammatory responses through alpha1beta1 integrin. Nature 2007; 446(7136): 680–684
26. You T, Zhu Z, Zheng X, Zeng N, Hu S, Liu Y, Ren L, Lu Q, Tang C, Ruan C, Zhang Y, Zhu L. Serum semaphorin 7A is associated with the risk of acute atherothrombotic stroke. J Cell Mol Med 2019; 23(4): 2901–2906
27. Lyu X, Liu X, Gong H, Liu Y, Zhou Z, Hu M, Zhang X. Serum Sema7A is increased in patients with acute aortic dissection. Expert Rev Mol Diagn 2023; 23(11): 1027–1035
28. Li M, Wu L, Wen Y, Wang A, Zhou X, Ren L, Lu Q, Li F, Zhu L, Tang C. Dysregulated cholesterol uptake and efflux of bone marrow-derived alpha-SMA^{+} macrophages contribute to atherosclerotic plaque formation. Cell Mol Life Sci 2025; 82(1): 134
29. Nakamura R, Sene A, Santeford A, Gdoura A, Kubota S, Zapata N, Apte RS. IL10-driven STAT3 signalling in senescent macrophages promotes pathological eye angiogenesis. Nat Commun 2015; 6(1): 7847
30. Schirmer SH, Fledderus JO, van der Laan AM, van der Pouw-Kraan TC, Moerland PD, Volger OL, Baggen JM, Bohm M, Piek JJ, Horrevoets AJ, van Royen N. Suppression of inflammatory signaling in monocytes from patients with coronary artery disease. J Mol Cell Cardiol 2009; 46(2): 177–185
31. Tamagnone L, Artigiani S, Chen H, He Z, Ming GI, Song H, Chedotal A, Winberg ML, Goodman CS, Poo M, Tessier-Lavigne M, Comoglio PM. Plexins are a large family of receptors for transmembrane, secreted, and GPI-anchored semaphorins in vertebrates. Cell 1999; 99(1): 71–80
32. Tóth E, Erdodi F, Kiss A. Myosin phosphatase is implicated in the control of THP-1 monocyte to macrophage differentiation. Int J Mol Sci 2021; 22(5): 2516
33. Peng H, Sun F, Jiang Y, Guo Z, Liu X, Zuo A, Lu D. Semaphorin 7a aggravates TGF-beta1-induced airway EMT through the FAK/ERK1/2 signaling pathway in asthma. Front Immunol 2023; 14: 1167605
34. Körner A, Bernard A, Fitzgerald JC, Alarcon-Barrera JC, Kostidis S, Kaussen T, Giera M, Mirakaj V. Sema7A is crucial for resolution of severe inflammation. Proc Natl Acad Sci USA 2021; 118(9): e2017527118
35. Wu X, Meng Y, Wang C, Yue Y, Dong C, Xiong S. Semaphorin7A aggravates coxsackievirusB3-induced viral myocarditis by increasing alpha1beta1-integrin macrophages and subsequent enhanced inflammatory response. J Mol Cell Cardiol 2018; 114: 48–57
36. Parkash J, Messina A, Langlet F, Cimino I, Loyens A, Mazur D, Gallet S, Balland E, Malone SA, Pralong F, Cagnoni G, Schellino R, De Marchis S, Mazzone M, Pasterkamp RJ, Tamagnone L, Prevot V, Giacobini P. Semaphorin7A regulates neuroglial plasticity in the adult hypothalamic median eminence. Nat Commun 2015; 6(1): 6385
37. Huntington KE, Carlsen L, So EY, Piesche M, Liang O, El-Deiry WS. Integrin/TGF-beta1 inhibitor GLPG-0187 blocks SARS-CoV-2 Delta and Omicron pseudovirus infection of airway epithelial cells *in vitro*, which could attenuate disease severity. Pharmaceuticals (Basel) 2022; 15(5): 618
38. MacDonald WJ, Verschleiser B, Carlsen L, Huntington KE, Zhou L, El-Deiry WS. Broad spectrum integrin inhibitor GLPG-0187 bypasses immune evasion in colorectal cancer by TGF-beta signaling mediated downregulation of PD-L1. Am J Cancer Res 2023; 13(7): 2938–2947